

Enhanced mechanical and thermal properties of two-dimensional SiC and GeC with temperature and size dependence

Lei Huang(黄磊), Kai Ren(任凯), Huanping Zhang(张焕萍), and Huasong Qin(覃华松)
Citation: Chin. Phys. B, 2023, 32 (**7**): 076103. DOI: 10.1088/1674-1056/acc78f
Journal homepage: http://cpb.iphy.ac.cn; http://iopscience.iop.org/cpb

What follows is a list of articles you may be interested in

Effects of atomic corrugations on electronic structures in $Pb_{1-x}Bi_x$ thin films

Pengju Li(李鹏举), Kun Xie(谢鹍), Yumin Xia(夏玉敏), Desheng Cai(蔡德胜), and Shengyong Qin(秦胜勇)
Chin. Phys. B, 2023, 32 (**6**): 066101. DOI: 10.1088/1674-1056/acbf29

Fabrication of honeycomb AuTe monolayer with Dirac nodal line fermions

Qin Wang(汪琴), Jie Zhang(张杰), Jierui Huang(黄杰瑞), Jinan Shi(时金安), Shuai Zhang(张帅), Hui Guo(郭辉), Li Huang(黄立), Hong Ding(丁洪), Wu Zhou(周武), Yan-Fang Zhang(张艳芳), Xiao Lin(林晓), Shixuan Du(杜世萱), and Hong-Jun Gao(高鸿钧)
Chin. Phys. B, 2023, 32 (**1**): 016102. DOI: 10.1088/1674-1056/aca14a

First-principles study of a new BP_2 two-dimensional material

Zhizheng Gu(顾志政), Shuang Yu(于爽), Zhirong Xu(徐知荣), Qi Wang(王琪), Tianxiang Duan(段天祥), Xinxin Wang(王鑫鑫), Shijie Liu(刘世杰), Hui Wang(王辉), and Hui Du(杜慧)
Chin. Phys. B, 2022, 31 (**8**): 086107. DOI: 10.1088/1674-1056/ac5a40

Radiation effects of electrons on multilayer $FePS_3$ studied with laser plasma accelerator

Meng Peng(彭猛), Jun-Bo Yang(杨俊波), Hao Chen(陈浩), Bo-Yuan Li(李博源), Xu-Lei Ge(葛绪雷), Xiao-Hu Yang(杨晓虎), Guo-Bo Zhang(张国博), and Yan-Yun Ma(马燕云)
Chin. Phys. B, 2022, 31 (**8**): 086102. DOI: 10.1088/1674-1056/ac5c34

Substitutions of vertex configuration of Ammann-Beenker tiling in framework of Ammann lines

Jia-Rong Ye(叶家容), Wei-Shen Huang(黄伟深), and Xiu-Jun Fu(傅秀军)
Chin. Phys. B, 2022, 31 (**8**): 086101. DOI: 10.1088/1674-1056/ac5981

SPECIAL TOPIC — Smart design of materials and design of smart materials

Enhanced mechanical and thermal properties of two-dimensional SiC and GeC with temperature and size dependence

Lei Huang(黄磊)[1], Kai Ren(任凯)[1,†], Huanping Zhang(张焕萍)[1], and Huasong Qin(覃华松)[2,‡]

[1] *School of Mechanical and Electronic Engineering, Nanjing Forestry University, Nanjing* 210037, *China*

[2] *Laboratory for Multiscale Mechanics and Medical Science, SV LAB, School of Aerospace, Xi'an Jiaotong University, Xi'an* 710049, *China*

(Received 4 January 2023; revised manuscript received 23 March 2023; accepted manuscript online 25 March 2023)

Two-dimensional materials with novel mechanical and thermal properties are available for sensors, photodetectors, thermoelectric, crystal diode and flexible nanodevices. In this investigation, the mechanical and thermal properties of pristine SiC and GeC are explored by molecular dynamics simulations. First, the fracture strength and fracture strain behaviors are addressed in the zigzag and armchair directions at 300 K. The excellent toughness of SiC and GeC is demonstrated by the maximal fracture strain of 0.43 and 0.47 in the zigzag direction, respectively. The temperature-tunable tensile strength of SiC and GeC is also investigated. Then, using non-equilibrium molecular dynamics (NEMD) calculations, the thermal performances of SiC and GeC are explored. In particular, the thermal conductivity of SiC and GeC shows a pronounced size dependence and reaches up to 85.67 $W{\cdot}m^{-1}{\cdot}K^{-1}$ and 34.37 $W{\cdot}m^{-1}{\cdot}K^{-1}$, respectively. The goal of our work is to provide a theoretical framework that can be used in the near future. This will enable us to design an efficient thermal management scheme for two-dimensional materials in electronics and optoelectronics.

Keywords: two-dimensional, molecular dynamics, mechanical property, heat transport

PACS: 61.46.–w **DOI:** 10.1088/1674-1056/acc78f

1. Introduction

By using a micromechanical stripping method, graphene has been successfully separated.[1] Due to their remarkable characteristics and numerous possible applications, two-dimensional (2D) materials have garnered extensive attention and research interest.[2,3] For example, graphene has excellent electronic,[4] thermal,[5,6] catalytic,[7] mechanical[8] and magnetic[9] properties. Single-layer graphene's bipolar electric field effect demonstrates that the charge carriers are more mobile than in semiconductors.[10] Graphene also has high thermoelectric power[10,11] and excellent nonlinear optical characteristics combined with fast response and wide wavelength range in optoelectronic and photonic applications.[12] Inspired by such exciting behaviors of graphene and its successful application in various advanced nanotechnology, research on other 2D materials has been explored.[13] Although they present a large specific surface area, these graphene-like materials possess different mechanical, thermal, electrical, optical and catalytic properties.[14–16]

The electronic, mechanical and thermal performances of the 2D materials have a critical role in the development of atomic devices. For instance, the mechanical properties of borophene are highly anisotropic: in comparison to the armchair direction, the zigzag direction (also known as the buckled direction) has a substantially lower Young's modulus and fracture strength.[17] The thermal conductance of pure black and blue phosphorene nanoribbons is sensitively affected by edge shape and breadth, and they both have a distinctly anisotropic thermal performance.[18] The mechanical properties of MoS_2 can determine the fracture strength and fracture strain of MoS_2/WSe_2 lateral heterostructures. These properties are highly temperature sensitive, and when compared to the graphene–hBN heterostructure, the MoS_2/WSe_2 heterostructure exhibits an order of magnitude lower interfacial thermal conductivity.[19] The properties of materials with negative Poisson's ratio are very necessary for many advanced applications because they typically have enhanced toughness and shear resistance, along with enhanced sound and vibration absorption, such as the puckered atomic structure of single-layer black phosphorus and B_4N monolayer material. Materials that have a negative Poisson ratio are named auxetic materials. They represent an exciting prospect for enhancing mechanical properties and are necessary for many advanced applications. For example, the Poisson ratios of the puckered atomic structure of black phosphorus[20] and B_4N[21] are calculated as -0.267 and -0.032, respectively, and these materials can be considered for future nanomechanical devices. Additionally, due to their excellent properties, silicon carbide (SiC) and germanium carbide (GeC) have garnered a lot of interest.[22,23] SiC possesses a large bandgap of about 3.354 eV,[24] a high saturation electron drift velocity (3×10^7 cm/s), a strong electric breakdown field (3×10^6 V/cm), and is used in high-temperature devices suitable for DC to microwave frequencies.[25] SiC is also a potential electromag-

†Corresponding author. E-mail: kairen@njfu.edu.cn

‡Corresponding author. E-mail: huasongqin@xjtu.edu.cn

© 2023 Chinese Physical Society and IOP Publishing Ltd

netic shielding material and it can be used for electronic packaging of highly integrated circuits, wireless communication, electronic base stations and other electronic equipment.[26,27] Besides, the defects in a SiC monolayer can induce a sizeable spin effect and strong spin–phonon coupling.[28] Furthermore, GeC also acts as a semiconductor with a bandgap of about 2.515 eV,[22] indicating that it is a promising candidate for application in semiconductor devices, crystal diodes, and photovoltaic systems.[29] Due to the exceptional optical performance of 2D GeC, it has undergone substantial research for prospective use in heterostructure devices and solar cells.[30] In comparison to graphene, the mechanical characteristics of a GeC monolayer indicate a low in-plane stiffness (143.8 N/m) and a high Poisson ratio (0.281).[31] Although there have been a large number of studies on the applications of tSiC and GeC monolayers, their mechanical and thermal characteristics are rarely reported and these are crucial properties to explore for further advanced functional nanodevices.

To explore the mechanical characteristics of SiC and GeC monolayers under uniaxial stress in the armchair and zigzag directions, we conduct molecular dynamics simulations (MD) in this work. The impacts of temperature and already-existing fractures on mechanical characteristics are discussed. Additionally, the heat transport capabilities of SiC and GeC monolayers are investigated. Adjustable mechanical and thermal characteristics of SiC and GeC monolayers point to possible usage in nanodevices.

2. Simulation methods

In our work, the zigzag and armchair directions of the SiC and GeC monolayers are oriented along the x and y directions, respectively, as shown in Fig. 1. Both the zigzag and armchair directions use periodic boundary conditions, which means a nanosheet structure is obtained. The Large-scale Atomic/Molecular Massively Parallel Simulator (LAMMPS) was used for all MD simulations.[32] It uses OVITO software for structural visualization.[33] To ensure the stability of the values and the correctness of the energy conservation, the time step of all MD simulations is set to 1.0 fs. Initially, the whole system is relaxed at a constant temperature and constant pressure for 200 ps through the Nose–Hoover thermostat. The Tersoff potential, which is often employed and taken into consideration owing to correct parameterization, is utilized to represent the interatomic interactions to achieve agreement with the DFT computations and experimental data.

In the mechanical calculations, all the simulations are performed using a 194.5 Å×198.1 Å supercell that contains periodic boundary conditions applied in any direction along the plane. Here, the fix/deform method as defined in LAMMPS is used to apply in-plane uniaxial tension with a strain rate of 2×10^8 s^{-1}. The system's temperature is maintained at a constant level during the tensile deformation process, while the other directions are maintained at zero pressure. During the MD simulations, we examine the normal corresponding forces in the zigzag and armchair directions to obtain the mechanical properties of the two material structures.

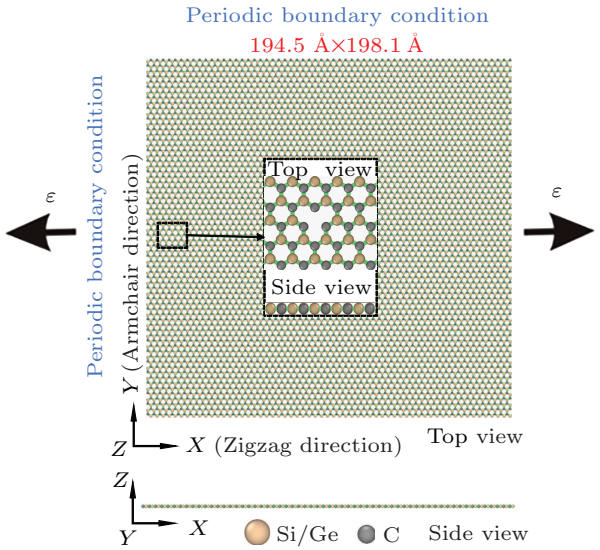


Fig. 1. The tensile simulation model of the SiC (or GeC) monolayers with dimensions of 194.5 Å×198.1 Å. The figure shows the top and side views, and the zoomed-in views (top and side views) of the interface. Both zigzag and armchair directions use periodic boundary conditions.

Non-equilibrium molecular dynamics (NEMD) simulations are used in the thermal simulations to calculate the thermal conductivity with the length and the width of the SiC (or GeC) monolayers at about 200.23 Å and 99.09 Å, respectively. The studied system was first equilibrated with an NPT ensemble for 100 ps and then the system was relaxed with an NVE ensemble for 2000 ps. The kinetic energy of the hottest atom in the heat sink slab and the coldest atom in the heat source slab are exchanged for 6 ns to produce the heat flux (J).

3. Results and discussion

3.1. Mechanical behavior

Structural integrity is maintained after the total relaxation of the SiC and GeC monolayers, suggesting thermal stability. Next, we investigate the zigzag and armchair direction fracture behaviors of the SiC and GeC monolayers under tensile pressure at 300 K. The obtained deformation and initial crack of the SiC and GeC monolayers are shown in Figs. 2(a) and 2(b), where one can see that the atomic stress near the crack has been released, and the fracture strains of SiC and GeC along the zigzag direction are larger than those along the armchair one. Furthermore, the fracture strength of SiC is greater than GeC in both directions, and conversely, the maximal strain that GeC can withstand is greater than SiC in both directions, which is demonstrated by the stress–strain curve of SiC and GeC in Fig. 3.

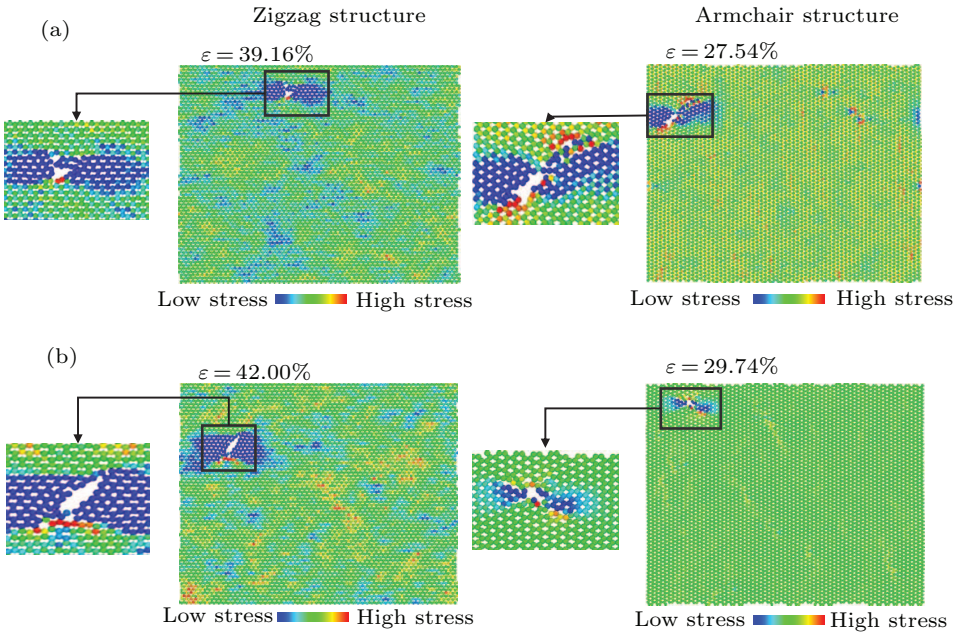


Fig. 2. Deformation and initial crack of zigzag and armchair (a) SiC and (b) GeC structures under tensile loading. The color contour in the image shows how the normal stress is distributed along the direction of tensile tension.

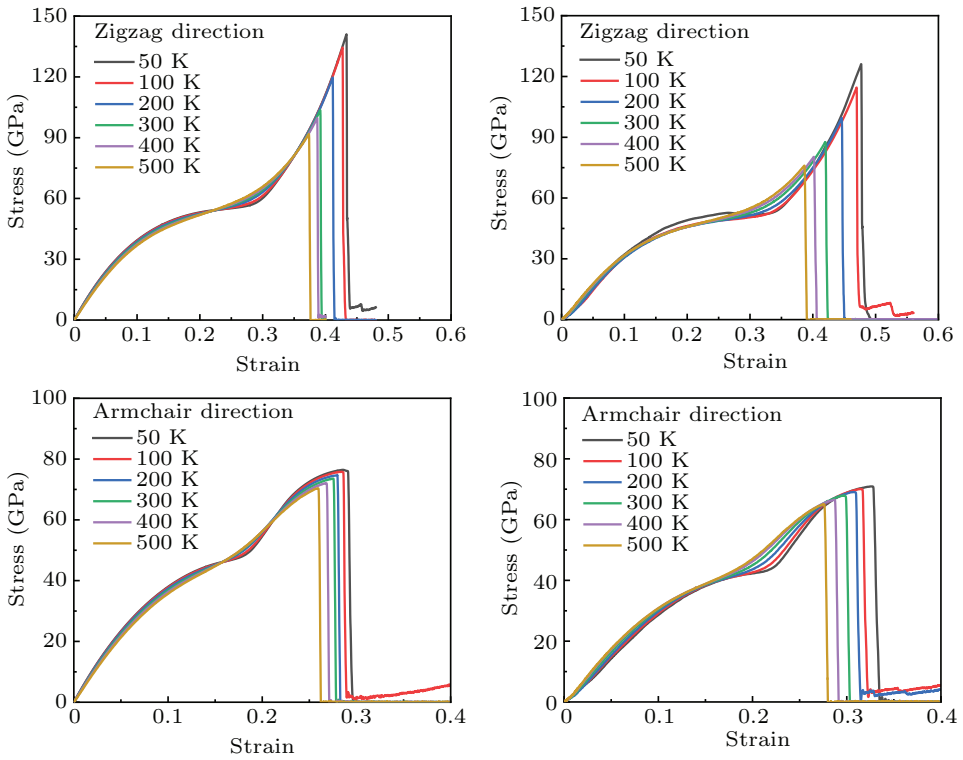


Fig. 3. The mechanical characteristics of SiC and GeC structures: the stress–strain curves for SiC (a), (c) and GeC (b), (d) in the zigzag (a), (b) and armchair (c), (d) directions.

In Fig. 3, it can be seen that the strain in SiC increases from 0 to 39.16% along the zigzag direction, corresponding to the stress increasing from 0 to 103.55 GPa. At the same time, the strain increasing from 0 to 27.54% can induce stress increases from 0 to 73.59 GPa along the armchair direction. Besides, when an external strain is applied to GeC in the zigzag (armchair) direction of up to 42% (29.74%), the stress increases will increase to 87.64 GPa (67.9 GPa). As shown in the stress–strain curves, both materials exhibit much greater zigzag fracture strengths and strain than armchair fracture strengths and strain, indicating anisotropy in their mechanical properties. The strongest 2D material is graphene, which has a fracture strength of 100–130 GPa and a Young's modulus of about 1.0 TPa.[34] On comparison, SiC and GeC are much weaker than graphene but far more robust than other 2D materials, such as borophene (23.45–55.9 GPa),[19] silicene (12.5 GPa)[35] and MoS_2 (11–13 GPa).[17] The effect of temperature on the stress–strain curves of SiC and GeC is also

addressed in Fig. 3. One can see that SiC and GeC behave mechanically similarly in zigzag (or armchair) directions at various temperatures before fracture, which means that the temperature mainly changes the ultimate fracture performance.

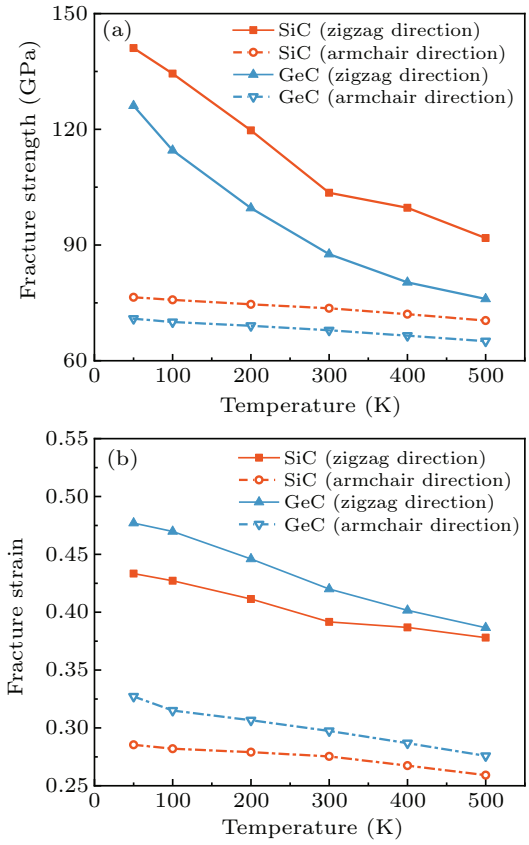


Fig. 4. Trends of (a) fracture strength and (b) fracture strain at different temperatures for SiC and GeC.

Then, we investigated the effect of the mechanical characteristics of the SiC and GeC monolayers at different temperatures. The fracture strength and strain of SiC and GeC possess an obvious dependence on the temperature between 50 K and 500 K, as shown in Fig. 4. Besides, nonlinear elastic behavior is observed for SiC and GeC. As shown in Fig. 4(a), as the temperature rises, both the fracture strength and fracture strain of SiC (or GeC) considerably decline. In more detail, the fracture strength of SiC reduces by 42.5% and 41.59% in zigzag and armchair directions, respectively, when the temperature rises from 50 K to 500 K. The fracture strength of GeC along the zigzag and armchair directions are likewise reduced by around 41.69% and 39.27%, respectively. In addition, the fracture strain of the SiC decreases by 71.2% and 56.9% for zigzag and armchair directions, respectively, while the GeC reduces by about 70.1% and 59.2% along zigzag and armchair directions, respectively. All of these results show that SiC and GeC are more temperature sensitive in terms of their fracture strength in a zigzag direction. At higher temperatures, the vibrations of atoms are greater, and it is easier for local chemical bonds to attain critical bond lengths and break as a result. This phenomenon is known as temperature-induced softening. This resembles the mechanical characteristics of certain common 2D materials, such as MoS_2,[36] graphene[34] and silicene,[35] at different temperatures.

Defect engineering is a common technique to modify the characteristics of 2D materials,[6,37,38] and defects also can be introduced easily in SiC and GeC during their fabrication processes. Thus, the response of the mechanical behaviors of SiC and GeC to the initial crack is investigated along zigzag and armchair directions, as shown in Fig. 5. We perform MD simulations at 300 K and the obtained fracture strain and fracture strength for various crack lengths (L) in SiC and GeC, ranging up to 5 nm, are shown in Figs. 5(a) and 5(b), respectively. Interestingly, SiC and GeC fracture strengths can be significantly reduced by a pre-existing crack in both zigzag and armchair orientations. Evidently, the shorter crack length can tune the fracture strength and strain of the SiC and GeC more effectively.

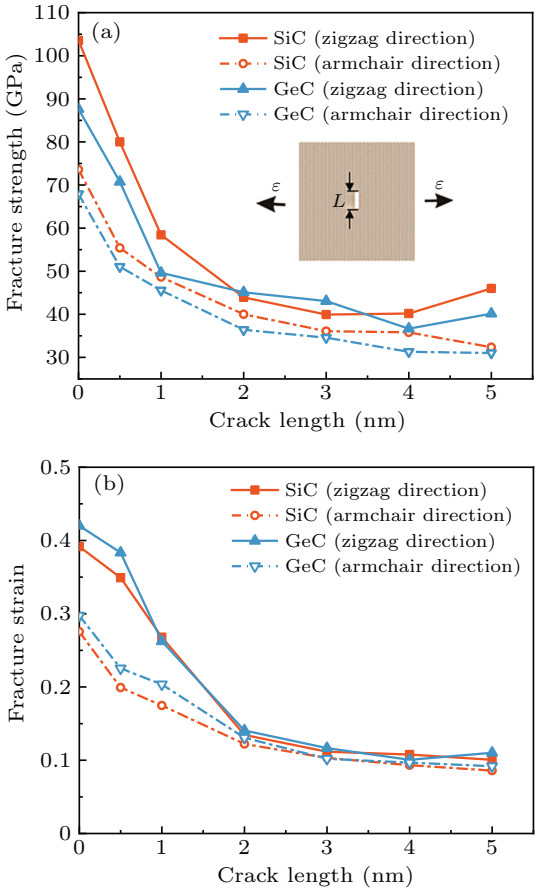


Fig. 5. (a) Schematic of applied stress on SiC (or SiC) with defective structure; the calculated (b) fracture strength and (c) the fracture strain of the SiC and GeC as a function of crack length (L) under tensile loading.

3.2. Thermal properties

The SiC and GeC monolayers possess semiconductor characteristics, suggesting desirable applications in nanoelectronics and thermoelectric devices, therefore, their heat transport properties are also critical. The thermal conductivities of SiC and GeC are discussed using NEMD simulations. As shown in Fig. 6(a), both ends of the SiC (or GeC) mono-

layer are fixed, and hot and cold baths are located near the fixed parts. Thus, the heat flux is along the x direction. The thermal properties in zigzag and armchair directions are investigated by setting them as the x direction. The temperature profiles, after reaching a steady state, of SiC and GeC in the zigzag direction are demonstrated in Fig. 6(b). For pure SiC and GeC, by fitting the linear area (depicted by a straight line) on the temperature profile, the temperature gradient ($\mathrm{d}T/\mathrm{d}x$) is derived. Following that, Fourier's law is used to compute the thermal conductivity (κ)

$$\kappa = \frac{J}{A\mathrm{d}T/\mathrm{d}x}, \tag{1}$$

where A represents the region in cross-section through which the heat flux flows. In order to obtain the thermal conductivity at room temperature (300 K), the hot and cold baths fixed at both ends in Fig. 6(a) were set to 320 K and 280 K, respectively. Therefore, the thermal conductivity of pure SiC at a temperature of 300 K is calculated as 16.89 $\mathrm{W{\cdot}m^{-1}{\cdot}K^{-1}}$ and 18.99 $\mathrm{W{\cdot}m^{-1}{\cdot}K^{-1}}$ along the zigzag and armchair directions, respectively, which are higher than those of transition metal dichalcogenides materials, such as MoS_2 (5.93 $\mathrm{W{\cdot}m^{-1}{\cdot}K^{-1}}$) and WSe_2 (7.09 $\mathrm{W{\cdot}m^{-1}{\cdot}K^{-1}}$).[19] Additionally, pure GeC has a thermal conductivity of 3.89 $\mathrm{W{\cdot}m^{-1}{\cdot}K^{-1}}$ in the zigzag direction and 4.49 $\mathrm{W{\cdot}m^{-1}{\cdot}K^{-1}}$ in the armchair direction. Compared to BCN, which has a thermal conductivity of 28–46 $\mathrm{W{\cdot}m^{-1}{\cdot}K^{-1}}$, SiC and GeC exhibit a much lower thermal conductivity.[39]

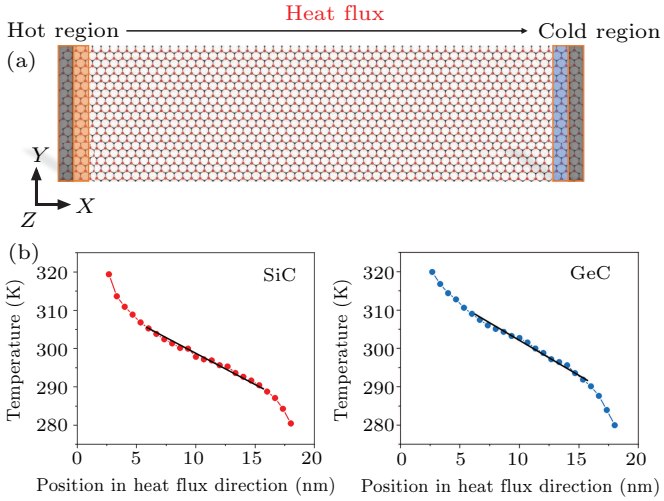


Fig. 6. (a) Schematic diagram of the heat transfer model and (b) the calculated temperature profiles of pure SiC and GeC monolayers along the zigzag direction.

Then, to explore the effect of size on the tunable thermal property of SiC and GeC, we fixed the value of the width and changed the length from 200 Å to 2000 Å at 300 K. The calculated thermal property of SiC and GeC with different lengths is given in Fig. 7(a), which shows that the thermal conductivity of SiC sheet increases from 16.89 $\mathrm{W{\cdot}m^{-1}{\cdot}K^{-1}}$ to 85.67 $\mathrm{W{\cdot}m^{-1}{\cdot}K^{-1}}$ along the zigzag direction and from 18.99 $\mathrm{W{\cdot}m^{-1}{\cdot}K^{-1}}$ to 82.79 $\mathrm{W{\cdot}m^{-1}{\cdot}K^{-1}}$ along the armchair direction. The thermal conductivity of pure GeC sheet is enhanced from 3.89 $\mathrm{W{\cdot}m^{-1}{\cdot}K^{-1}}$ to 34.37 $\mathrm{W{\cdot}m^{-1}{\cdot}K^{-1}}$ along the zigzag direction and from 4.49 $\mathrm{W{\cdot}m^{-1}{\cdot}K^{-1}}$ to 32.74 $\mathrm{W{\cdot}m^{-1}{\cdot}K^{-1}}$ along the armchair direction. These results indicate an obvious size dependence of the thermal property of SiC and GeC.

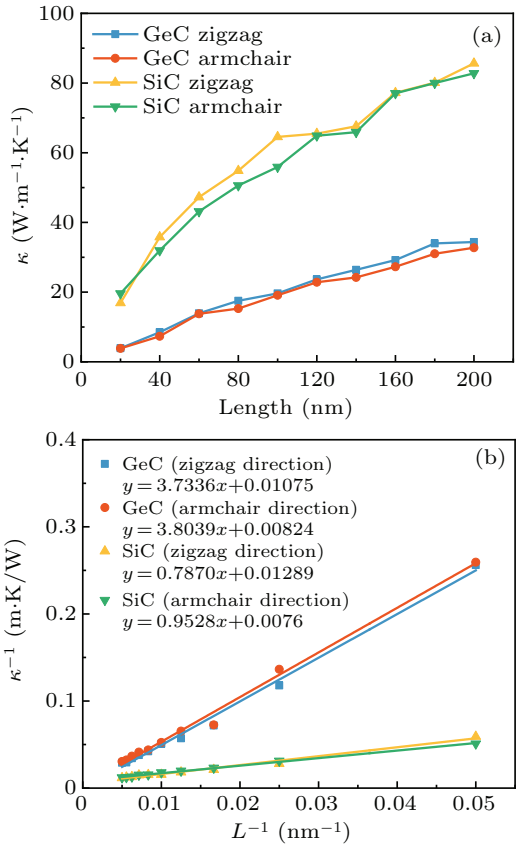


Fig. 7. (a) Thermal conductivity measured in pure SiC and GeC at various lengths; (b) the relationships between the inverse thermal conductivity and the inverse sample length for pure SiC and GeC.

When the length of the 2D material is shorter than the phonon mean free path (MFP), which is a common approach to optimizing the heat transport performance of 2D materials, the system size has a significant impact on the thermal conductivity of these materials.[40] The following connection between the inverse thermal conductivity and the inverse sample length L^{-1} are used to calculate the effective MFP:[41]

$$\kappa^{-1} = \kappa_{\infty}^{-1}\left(\frac{l}{L}+1\right), \tag{2}$$

where l is MFP and κ_{∞} is the thermal conductivity of an infinitely long sample. From the fitting curve shown in Fig. 7(b), the obtained effective MFPs for pure SiC and GeC are 109.97 nm and 321.21 nm, respectively. The thermal conductivity of a pure SiC (GeC) infinite-length sample is 126.46 $\mathrm{W{\cdot}m^{-1}{\cdot}K^{-1}}$ (85.30 $\mathrm{W{\cdot}m^{-1}{\cdot}K^{-1}}$).

Besides, we also calculate the thermal property of SiC and GeC at different temperatures ranging from 100 K to 500 K, as shown in Fig. 8(a). One can see that the thermal conductivity of both SiC and GeC in the zigzag and the armchair

directions are still almost the same, and the simulation results of SiC show that its thermal conductivity decreases from 29.50 $W{\cdot}m^{-1}{\cdot}K^{-1}$ to 13.92 $W{\cdot}m^{-1}{\cdot}K^{-1}$ along the zigzag direction, and from 28.60 $W{\cdot}m^{-1}{\cdot}K^{-1}$ to 15.23 $W{\cdot}m^{-1}{\cdot}K^{-1}$ along the armchair direction, indicating a negative temperature dependence. However, the thermal conductivity of GeC shows no significant difference with temperature. The obtained tunable thermal property of SiC and GeC suggests a promising use for thermoelectric applications.

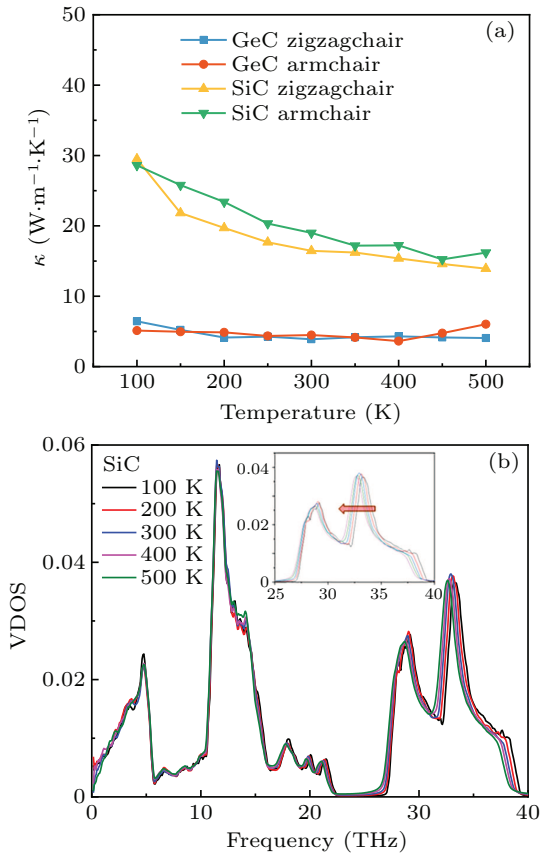


Fig. 8. (a) Thermal conductivity of pure SiC and GeC with different temperatures. (b) Calculated VDOS for the SiC monolayer along the zigzag direction at temperatures of 100 K to 500 K.

In Fig. 8(a), the SiC monolayer shows a strong temperature-dependent thermal conductivity, which is related to phonon anharmonicity. To explore the potential physical mechanism of temperature-dependent thermal conductivity in the SiC monolayer, we calculate the vibrational density of states (VDOS) in the SiC monolayer at 100–500 K from

$$\mathrm{VDOS}(\omega) = \frac{1}{\sqrt{2\pi}} \int_0^{\infty} \mathrm{e}^{\mathrm{i}\omega T} C(t)\,\mathrm{d}t, \tag{3}$$

where ω is the angular frequency and $C(t)$ represents the velocity autocorrelation function. For total VDOS, $C(t) = \langle \sum_{j=1}^{N} \bar{v}_j(0) \cdot \bar{v}_j(t) \rangle$, where $\bar{v}_j(t)$ is the velocity of atom j and the symbol $\langle\ \rangle$ represents the ensemble average.[42] The calculated results are shown as Fig. 8(b) with the phonon frequency ranging from 0 to 40 THz. The peak frequency for the SiC monolayer at 300 K is around 11.5 THz. The peak value of VDOS near 25–40 THz varies significantly with temperature, thus, we focus on this range. As shown in Fig. 8(b), the increased temperature causes a significant redshift in the high frequency peaks of SiC, induced by an enhanced phonon anharmonicity, reducing the thermal conductivity and therefore exhibiting a temperature dependence. This phenomenon has also been explored in Janus MoSSe and WSSe monolayers.[43] Our simulations are an important reference for the future development of thermal devices and thermoelectric energy conversion.

4. Conclusion and perspectives

In this study, molecular dynamics simulations were used to systematically examine the in-plane mechanical and thermal transport characteristics of pure SiC and GeC. Both SiC and GeC demonstrate an excellent toughness with fracture strain of about 0.43 and 0.47 in the zigzag direction at 300 K, respectively, which can be decreased by temperature and the introduced crackle. Furthermore, the thermal conductivities of pure SiC (GeC) are calculated as 16.89 $W{\cdot}m^{-1}{\cdot}K^{-1}$ (3.89 $W{\cdot}m^{-1}{\cdot}K^{-1}$) and 18.99 $W{\cdot}m^{-1}{\cdot}K^{-1}$ (4.49 $W{\cdot}m^{-1}{\cdot}K^{-1}$) along zigzag and armchair directions, respectively, by a non-equilibrium molecular dynamics method. Additionally, the thermal conductivity of SiC (GeC) can reach 85.67 $W{\cdot}m^{-1}{\cdot}K^{-1}$ (34.37 $W{\cdot}m^{-1}{\cdot}K^{-1}$) due to a size effect, although an increase in temperature will reduce that. The obtained size and temperature-tunable mechanical and thermal characteristics of SiC and GeC suggest promising applications as thermoelectric and flexible nanodevices.

Acknowledgements

All the authors would like to thank the support of the Natural Science Foundation of Jiangsu (Grant No. BK20220407), the National Natural Science Foundation of China (Grant Nos. 12102323, 11890674), the China Postdoctoral Science Foundation (Grant No. 2021M692574), and the Fundamental Research Funds for the Central Universities (Grant No. sxzy012022024). This work is also supported by the HPC Center, Nanjing Forestry University, China.

References

[1] Geim A K and Novoselov K S 2007 *Nat. Mater.* **6** 183
[2] Jariwala D, Sangwan V K, Lauhon L J, Marks T J and Hersam M C 2013 *Chem. Soc. Rev.* **42** 2824
[3] Wu R, Zhu R Z, Zhao S H, Zhang G, Tian H and Ren T L 2021 *Science China Information Sciences* **64** 140401
[4] Medeiros P V C, Stafström S and Björk J 2014 *Phys. Rev. B* **89** 041407
[5] Yu C and Zhang G 2013 *J. Appl. Phys.* **113** 044306
[6] Qin H. Chen Y, Wu Y, Li M, Liu Y and Pei Q X 2022 *J. Phys. Chem. C* **126** 5759
[7] Fei H, Dong J, Arellano-Jimenez M J, Ye G, Dong Kim N, Samuel E L, Peng Z, Zhu Z, Qin F, Bao J, Yacaman M J, Ajayan P M, Chen D and Tour J M 2015 *Nat. Commun.* **6** 8668
[8] Cadelano E and Colombo L 2012 *Phys. Rev. B* **85** 245434
[9] Santos E J G, Sánchez-Portal D and Ayuela A 2010 *Phys. Rev. B* **81** 125433

[10] Castro Neto A H, Guinea F, Peres N M R, Novoselov K S and Geim A K 2009 *Rev. Mod. Phys.* **81** 109

[11] Sang M, Shin J, Kim K and Yu K J 2019 *Nanomaterials* **9** 374

[12] Liu Z, Zhang X, Yan X, Chen Y and Tian J 2012 *Chinese Science Bulletin* **57** 2971

[13] Miro P, Audiffred M and Heine T 2014 *Chem. Soc. Rev.* **43** 6537

[14] Ren K, Ma X, Liu X, Xu Y, Huo W, Li W and Zhang G 2022 *Nanoscale* **14** 8463

[15] Zhang J, Zhang C, Ren K and Lin X 2022 *Nanotechnology* **33** 345705

[16] Ren, K, Yan Y, Zhang Z, Sun M and Schwingenschlögl U 2022 *Appl. Surf. Sci.* **604** 154317

[17] Sha Z D, Pei Q X, Zhou K, Dong Z and Zhang Y W 2018 *Extreme Mechanics Letters* **19** 39

[18] Cao W, Xiao H, Ouyang T, Wang Z and Xiong R 2019 *Phys. A* **383** 1493

[19] Qin H, Pei Q X, Liu Y and Zhang Y W 2019 *Phys. Chem. Chem. Phys.* **21** 15845

[20] Jiang J W and Park H S 2014 *Nat. Commun.* **5** 4727

[21] Wang B, Wu Q, Zhang Y, Ma L and Wang J 2019 *ACS Appl. Mater. Interfaces* **11** 33231

[22] Ren K, Sun M, Luo Y, Wang S, Xu Y, Yu J and Tang W 2019 *Phys. A* **383** 1487

[23] Li S, Sun M, Chou J P, Wei J, Xing H and Hu A 2018 *Phys. Chem. Chem. Phys.* **20** 24726

[24] Ren K, Ren C, Luo Y, Xu Y, Yu J, Tang W and Sun M 2019 *Phys. Chem. Chem. Phys.* **21** 9949

[25] Bondoux C, Prené P, Belleville P, Guillet F, Lambert S, Minot, B and Jérisian R 2005 *Journal of the European Ceramic Society* **25** 2795

[26] Yin X, Kong L, Zhang L, Cheng L, Travitzky N and Greil P 2014 *International Materials Reviews* **59** 326

[27] Widmann M, Lee S Y, Rendler T, Son N T, Fedder H, Paik S, Yang L P, Zhao N, Yang S, Booker I, Denisenko A, Jamali M, Momenzadeh S A, Gerhardt I, Ohshima T, Gali A, Janzen E and Wrachtrup J 2015 *Nat. Mater.* **14** 164

[28] Whiteley S J, Wolfowicz G, Anderson C P, Bourassa A, Ma H, Ye M, Koolstra G, Satzinger K J, Holt M V, Heremans F J, Cleland A N, Schuster D I, Galli G and Awschalom D D 2019 *Nat. Phys.* **15** 490

[29] Xu Z, Li Y, Li C and Liu Z 2016 *Appl. Surf. Sci.* **367** 19

[30] Soref R A 1996 *Journal of Vacuum Science & Technology A* **14** 913

[31] Peng Q, Liang C, Ji W and De S 2013 *Mechanics of Materials* **64** 135

[32] Thompson A P, H M Aktulga, R Berger, D S Bolintineanu, W M Brown, P S Crozier, P J in't Veld, A Kohlmeyer, S G Moore, T D Nguyen, R Shan, M J Stevens, J Tranchida, C Trott and S J Plimpton 2022 *Computer Physics Communications* **271** 108171

[33] Stukowski A 2010 *Modelling and Simulation in Materials Science and Engineering* **18** 015012

[34] Pei Q X, Zhang Y W and Shenoy V B 2010 *Carbon* **48** 898

[35] Pei Q X, Sha Z D, Zhang Y Y and Zhang Y W 2014 *J. Appl. Phys.* **115** 023519

[36] Xiong S and Cao G 2015 *Nanotechnology* **26** 185705

[37] Ren K, Liu X, Chen S, Cheng Y, Tang W and Zhang G 2020 *Adv. Funct. Mater.* **30** 2004003

[38] Liu X, Zhang G and Zhang Y W 2016 *Nano Lett.* **16** 4954

[39] Zhang Y Y, Pei Q X, Liu H Y and Wei N 2017 *Phys. Chem. Chem. Phys.* **19** 27326

[40] Zhang Z, Ouyang Y, Cheng Y, Chen J, Li N and Zhang G 2020 *Phys. Rep.* **860** 1

[41] Hu M and Poulikakos D 2012 *Nano Lett.* **12** 5487

[42] Grest G S, Nagel S R, Rahman A and Witten T A 1981 *J. Chem. Phys.* **74** 3532

[43] Qin H, Ren K, Zhang G, Dai Y and Zhang G 2022 *Phys. Chem. Chem. Phys.* **24** 20437